HHS Public Access

Author manuscript

Nat Med. Author manuscript; available in PMC 2017 March 01.

Published in final edited form as:

Nat Med. 2016 September ; 22(9): 1033–1042. doi:10.1038/nm.4169.

Augmented endothelial exocytosis of angiopoietin-2 resulting from CCM3-deficiency contributes to the progression of cerebral cavernous malformation

Huanjiao Jenny Zhou[#1,2], **Lingfeng Qin**[#1], **Haifeng Zhang**[#1], **Wenwen Tang**[1,3], **Weidong Ji**[2,4], **Yun He**[1,5], **Xiaoling Liang**[6], **Zongren Wang**[2], **Qianying Yuan**[1,3], **Alexander Vortmeyer**[1], **Derek Toomre**[7], **Germaine Fuh**[8], **Minghong Yan**[9], **Martin S. Kluger**[1,10], **Dianqing Wu**[1,3,#], and **Wang Min**[1,2,4,#]

[1]Interdepartmental Program in Vascular Biology and Therapeutics, Department of Pathology, Yale University School of Medicine, New Haven, CT

[2]Center for Translational Medicine, The First Affiliated Hospital, Sun Yat-sen University, Guangzhou, China

[3]Department of Pharmacology, Yale University School of Medicine, New Haven, CT

[4]Guangzhou Darron Medscience, Co. Ltd, Guangzhou, China

[5]Department of Toxicology, School of Public Health, Sun Yat-sen University of Medical Sciences, Guangzhou, China

[6]State Key Laboratory of Ophthalmology, Zhongshan Ophthalmic Center, Sun Yat-sen University, Guangzhou, China

[7]Department of Cell Biology, Yale University School of Medicine, New Haven, CT

[8]Department of Antibody Engineering, Genentech Inc, South San Francisco, CA

[9]Department of Molecular Oncology, Genentech Inc, South San Francisco, CA

[10]Department of Immunobiology, Yale University School of Medicine, New Haven, CT

[#] These authors contributed equally to this work.

Abstract

[#] Contacting corresponding author: Dr. Wang Min, Interdepartmental Program in Vascular Biology and Therapeutics, Department of Pathology, Yale University School of Medicine, 10 Amistad St., 401B, New Haven, CT 06520. Tel: 203-785-6047; Fax: 203-737-2293; wang.min@yale.edu and dan.wu@yale.edu.

ACCESSION CODES:
None.

AUTHOR CONTRIBUTIONS
H.J.Z., L.Q., H.Z. and W.M. conceived the study, designed experiments and wrote the manuscript; H.J.Z., L.Q., H.Z.. W.T., W.J., Y.H., Z. W., Q.Y. and M.S.K. performed experiments; W.J., G.F. and M.Y. generated the anti-Angiopoietin-2 antibodies; X.L. interpreted retinal data; A.V. provided the human CCM blocks; and H.J.Z., L.Q., H.Z., D. T., D.W. and W.M. interpreted data. M.S.K edited the manuscript.

COMPETING FINANCIAL INTERESTS STATEMENT
None.

Cerebral cavernous malformations (CCMs) are vascular malformations that affect the central nervous system and result in cerebral hemorrhage, seizure and stroke. CCM arises from loss-of-function mutations in one of three genes: CCM1, CCM2 and CCM3 (PDCD10). CCM3 mutations in human often result in a more severe form of the disease, and CCM3 knockout mice show severe phenotypes with yet-to-be defined mechanisms. We have recently reported that CCM3 regulates UNC13 family-mediated exocytosis. Here we investigate endothelial cells (EC) exocytosis in CCM disease progression. We find that CCM3 suppresses UNC13B/VAMP3-dependent exocytosis of angiopoietin-2 (ANGPT2) in brain endothelial cells. CCM3 ablation in EC augments exocytosis and secretion of ANGPT2, correlating with destabilized EC junctions, enlarged lumen formation, and endothelial cell-pericyte dissociations. UNC13B deficiency that blunts ANGPT2 secretion from EC or an ANGPT2 neutralization antibody normalizes the defects caused by CCM3 deficiency. More importantly, ANGPT2 neutralization antibody treatment or UNC13B deficiency blunts the CCM lesion phenotypes, including disruption of EC junctions, vessel dilation and pericyte dissociation, in the brains and retinas caused by endothelial cell-specific CCM3 inactivation. Our study reveals that enhanced secretion of ANGPT2 in endothelial cells contributes to the progression of the CCM disease, providing a novel therapeutic approach to treat this devastating pathology.

Keywords

Cerebral cavernous malformation (CCM); CCM3/PDCD10; exocytosis; angiopoietin-2; pericyte; endothelial cell junction

INTRODUCTION

Cerebral cavernous malformations (CCMs) consist of clusters of enlarged endothelial channels (‘caverns’) that are arranged back-to-back to form densely packed sinusoids with little or no intervening brain parenchyma[1,2]. These lesions lack pericytes (PCs) and elastic tissue, so the vessel walls are thin, leaky and lack sub-endothelial support and an intact basal lamina. Ultra-structural analysis has revealed decreased numbers of PCs, endothelial detachment from the basal lamina and ruptures in the luminal endothelium probably due to reduced/damaged intercellular junctions[3]. CCMs are almost exclusively found within the neurovasculature of the central nervous system (CNS, i.e. brain and retina)[4,5], where they result in increased risk for stroke, seizures and focal neurological deficits[1,2]. Currently, the only treatment for CCM is surgical resection.

CCMs can be sporadic or familial and more than 90% of patients with inherited autosomal dominant CCM carry loss of function mutations in one of three genes: *CCM1*[6], *CCM2*[7] and CCM3 (*PDCD10*)[8]. CCM has been thought to result from a two-hit mechanism, and biallelic somatic mutations in one of the CCM genes have been identified in endothelial cells (ECs) lining cavernous vessels of patients carrying germline mutations[9-11]. This has been recently confirmed in a mouse model[12]. Recently, postnatal inactivation of *Ccm* genes in EC was shown to induce CCM lesions in brain tissue. Importantly, the lesions are characterized by a single layer of dilated endothelium, closely resembling human CCM[13-17]. Human CCMs are associated with loss-of-function mutations in any one of the three *CCM* genes, likewise

knockout of any one of the *Ccm* genes in mice produces CCM, suggesting that there is an essential pathway involving all three proteins. This hypothesis is bolstered by the knowledge that all three proteins can be found in the same complex within the cell and mediating several common signaling pathways[16,18-20]. However, CCM3 might also act separately from CCM1 and CCM2, as its mutation often results in a more severe form of the disease[21], and *Ccm3* knockout mice show severe phenotypes with yet-to-be defined mechanism[13-17].

CCM3 may have distinct but converging cellular functions from those of the CCM1 and CCM2 complex. The GCKIII kinases (including STK24 and STK25) specifically associates with CCM3 and they function in the same pathway as CCM3 in cardiovascular development[22,23]. We have unexpectedly found that CCM3 and STK24 negatively regulate exocytosis[24]. Exocytosis is a process by which a cell directs the contents of secretory vesicles toward extracellular space. These membrane-bound vesicles contain soluble proteins to be secreted to the extracellular environment and membrane proteins and lipids that are sent to become contents of the cell membrane. Exocytic vesicles (also called granules) differ in size and content that are highly cell-type dependent. Exocytosis is accomplished by the fusion of secretory vesicles with the plasma membrane through the assembly of the soluble *N*-ethylmaleimide–sensitive factor (NSF) attachment protein receptor (SNARE) complex. Before membrane fusion, additional proteins mediate and regulate the initial interaction between the vesicles and the acceptor membrane. They include the plasma-membrane proteins syntaxins, synaptosomal-associated proteins (SNAPs), vesicle-associated membrane proteins (VAMPs), the Rab family of small GTPases, the exocyst, and numerous other regulatory proteins. Among these regulatory proteins is the UNC13 family of proteins, which consists of UNC13A-D[25]. UNC13B and D contain two separate Ca^{2+}-binding C2 domains (C2A and C2B), and UNC13 is involved in granule tethering to plasma membranes through the binding of its C2B domain to membrane lipids during granule docking and priming prior to vesicle fusion with the plasma membranes. Our mechanistic studies suggest that CCM3 and STK24, by inhibiting UNC13 family of exocytosis regulators, regulate exocytosis and neutrophil degranulation[24]. The exocytic machinery that drives vesicle trafficking and membrane fusion in ECs is similar to that found in neurons and neutrophils[26]. It is known that ECs contain the Weibel-Palade body (WPB), a type of the secretory vesicle releasing von Willebrand factor (vWF) and P-selectin during inflammation. Moreover, angiopoietin-2 (ANGPT2) are released from WPBs in ECs[27,28]. Importantly, ANGPTs (ANGPT1 and ANGPT2) are endothelial growth factors that bind to the tyrosine kinase receptor TIE-2, cooperatively regulating EC adherens junction-dependent vascular stability and blood vessel formation during angiogenesis[29]. Our observations that ANGPT2 is increased in both mouse and human CCM lesions prompted us to explore the role of the CCM3-UNC13 network in regulation of the release of ANGPT2 and its implication in CCM lesion development.

In the present study, we demonstrate that CCM3-ablated ECs augment UNC13-mediated exocytosis and secretion of ANGPT2, leading to destabilized EC junctions and CCM lesion formation. Our study reveals a novel mechanism by which CCM3 mutations contribute to the progression of the CCM disease and a potential new therapeutic modality for treating this disease.

RESULTS

Mice with EC-inducible *Ccm3* deletion develop CCM lesions

Feeding Cdh5-CreERT2:mT/mG pups with tamoxifen from postnatal (P)1 to P3, which induced mG (EGFP) expression specifically in vasculatures of all tissues including brain (**Supplementary Fig.1a**). We induced EC-specific deletion of *Ccm3* in Cdh5-CreERT2;*Pdc10*$^{fl/fl}$ pups immediately after birth (hereafter termed *Ccm3*^{ECKO}) (**Supplementary Fig.1b–c**). *Ccm3*^{ECKO}, but not WT (*Pdc10*$^{fl/fl}$) pups, rapidly developed CCM lesions with dilated capillaries in the cerebella of brains, with onset at P5 and large lesions evident at P10 (**Fig.1a**). No *Ccm3*^{ECKO} pups could survive beyond P15 (n>50). CCM lesions (>10,000 μm^2) were primarily detected inside the granule cell layers of cerebella of *Ccm3*^{ECKO} and the lesion sizes were drastically enlarged at P10 compared to P5 (**Fig.1a–c**). CCM lesions in humans are formed by enlarged and irregular blood vessels that often result in cerebral hemorrhage. FITC-dextran perfusion at P10 showed that FITC-dextran was constrained inside capillary beds of brains and retinas in WT mice, but was diffused to surrounding tissues in the cerebella of *Ccm3*^{ECKO} (**Fig.1d–f**). Evans Blue Dye permeability assay also showed increased cerebellum vascular leakage in *Ccm3*^{ECKO} mice (**Fig.1g**). Venous malformations were also detected at the periphery of the retinal vascular plexus (**Fig.1h–i**), but not in skin or liver, as visualized by isolectin and CD31 staining. The retinas in *Ccm3*^{ECKO} mice were leaky as indicated by hemorrhage in the freshly isolated retinas and by visualization with a FITC-dextran perfusion assay (**Supplementary Fig.2a–b**).

CCM lesions exhibit disrupted EC junctions with increased ANGPT2 expression

To determine how capillaries enlarge in *Ccm3*^{ECKO}, we examined EC junctions and EC-PC interactions within the lesions. The lesions in *Ccm3*^{ECKO} mice were characterized by a single layer of dilated endothelium with significantly reduced PC coverage, as seen in human CCM lesions (Fig.2a,c). EC-PC association visualized by gap junctional protein connexin-43 staining was also drastically attenuated (**Fig.2a,c**). Endothelial adherens junctions visualized by VE-cadherin were disorganized and markedly downregulated in the lesion areas compared to normal vessels in WT brains (**Fig.2b–c**). Similarly, tight junction coverage in the lesions visualized by claudin-5 was also drastically reduced (**Fig.2b–c**). ANGPT2, secreted by ECs, is classically considered as an ANGPT1 antagonist, counteracting the stabilizing action of ANGPT1 to increase EC permeability[30,31]. ANGPT2 was basally detected inside ECs of normal vessels in WT brain, but was highly upregulated in *Ccm3*^{ECKO} brain both inside the dilated vessels and outside the lesions (**Fig.2d**). ANGPT2 protein levels were drastically increased in cerebellum of *Ccm3*^{ECKO} mice as detected by ELISA. We also detected increased ANGPT2 in the retina but not in the lung tissues or blood (**Fig.2e**), consistent with lesion formation sites. Expression of ANGPT2 mRNA (but not that of ANGPT1 or TIE2) was increased weakly on P5 and strongly on P10 in the cerebellum of *Ccm3*^{ECKO} (**Fig.2f**). We unexpectedly detected increased TIE2 phosphorylation in *Ccm3*^{ECKO} brains by Western blot (**Fig.2g**), suggesting activation of ANGPT2-TIE2 signaling during CCM lesion development.

To determine if ANGPT2 upregulation has clinical relevance, we examined expression of ANGPT2 in human CCM3 lesions. We obtained paraffin blocks for 8 cases of human CCM3 lesions. Six of the samples contained typical CCM lesions and surrounding relatively normal tissues based on H&E staining, and the other 2 cases also showed severe vascular fibrosis (**Supplementary Fig.3a**). ANGPT2 and p-TIE2 staining were absent in normal brain areas, but were significantly upregulated in CCM lesions accompanied by disruption of EC junctions (**Fig.2h–i; Supplementary Fig.3b–e**).

CCM3 restrains ANGPT2 secretion and maintains EC junctions

To determine if CCM3 regulates ANGPT2 secretion via UNC13-dependent exocytosis in vascular ECs, we first examined the expression of UNC13 members in both mouse and human brain microvascular ECs (MBMVEC and HBMVEC). UNC13B, but not UNC13A, C or D, was the dominant UNC13 isoform expressed in mouse and human ECs detected by qRT-PCR (**Supplementary Fig.4a–b**). Moreover, UNC13B forms a complex with CCM3 and GCKIII member STK24 (**Fig.3a**). In addition, CCM3 was co-localized with the vesicle-associated membrane proteins VAMP3 and VAMP8 (**Fig.3b**). To directly determine if CCM3 regulates exocytosis in ECs, we used VAMP8 fused with a pH-sensitive fluorescent protein PHluorin to visualize fusion processes of individual exocytic vesicles under live-cell TIRF microscopy. HBMVECs were co-transfected with the PHluorin probe and a control siRNA or CCM3 siRNA in the presence or absence of an UNC13B siRNA, and the knockdown efficiency and specificity of these siRNAs were verified by qRT-PCR (**Supplementary Fig.4c**). Vesicle fusion events and kinetics were quantified for individual fusion events recorded in the time-lapse TIRF images. CCM3 silencing in HBMVECs increased exocytic fusion events without affecting the fusion kinetics; moreover, the increased fusion events were suppressed by co-silencing of UNC13B (**Fig.3c**).

We next examined the direct effect of CCM3 deletion on ANGPT2 expression and secretion in ECs. WT and CCM3-depleted mouse brain microvascular ECs (MBMVEC) were isolated[32] and reconstituted with CCM3-WT (1-212aa) or CCM3-N (a truncated mutant containing the N-terminal 1-95aa that was found in human patients) by lentiviral transduction. ANGPT2 release was increased in CCM3-depleted MBMVEC and was attenuated by a reconstitution of CCM3-WT, but not CCM3-N (**Supplementary Fig.4d**). Silencing of CCM3, but not CCM1 or CCM2, in HBMVEC caused a significant increase in ANGPT2 secretion from the cells. ANGPT2 release augmented by CCM3 silencing could be significantly suppressed by co-silencing UNC13B (**Fig.3d–e**). However, ANGPT2 mRNA (**Supplementary Fig.4c**) or total ANGPT2 protein (**Fig.3f**) was not significantly altered by the silencing of CCM3 or UNC13B. Increases in ANGPT2 secretion correlated with enhanced phospho-TIE2 in CCM3 knockdown ECs. However, total TIE2 and ANGPT1 proteins were not affected in these cells (**Fig.3f**). Consistent with previous findings that CCM3 stabilizes GCKIII kinases[33], CCM3 knockdown induced a reduction in STK24 in ECs. We tested cycloheximide (CHX) blockade on ANGPT2 release. As we reported previously[34], a labile protein VEGFR2 was drastically reduced upon CHX treatment at 2 h. Total ANGPT2, TIE2 and CCM3 proteins were reduced by CHX treatment after 8 h (**Supplementary Fig.4e**), suggesting that these proteins were relatively stable as CCM3 (half-life ≥ 8 h)[32]. Protein synthesis inhibition by CHX had no effects on the total or

secreted ANGPT2 in the control or CCM3 depleted ECs within the 8 h periods (Fig.3g). These data are consistent with previous notions that ANGPT2 is primarily produced by protein release[28]. We detected localization of ANGPT2 in VAMP3-positive vesicles in CCM3-knockdown ECs (**Supplementary Fig.4f**), Consistently, enhanced ANGPT2 secretion and phospho-TIE2 in CCM3 depleted ECs were also blunted by co-silencing VAMP3 (**Supplementary Fig.4g-h**). We observed a similar role of CCM3 in vWF release and P-selectin surface expression in ECs (**Supplementary Fig.4i–j**). These data demonstrate that CCM3 restrains exocytosis of ANGPT2 from the Weibel-Palade body in ECs.

We finally examined if CCM3-mediated ANGPT2 secretion contributes to EC junctions and EC integrity. CCM3 knockdown drastically disrupted both adherens and tight junctions as detected by immunostaining for VE-cadherin and ZO-1, respectively. However, co-silencing UNC13B or anti-ANGPT2 antibody significantly restored normal adherens junctions and tight junctions (**Fig.3h–i**). Co-silencing UNC13B or anti-ANGPT2 antibody also restored barrier function in the CCM3-ablated ECs as assessed for transendothelial electric resistance (TEER) by electrical cell-substrate impedance sensing (**Fig.3j**), which showed similar results to transendothelial flux measurements with FITC-dextrans[35].

CCM3-ANGPT2 axis regulates EC lumen formation and PC recruitment

To determine if CCM3 regulates vessel lumen diameters as observed in the *Ccm3*^{ECKO} brains, we analyzed EC sprouting and lumen formation using an optimized *in vitro* EC sprouting and tube formation model[36,37]. EGFP-expressing and/or siRNAs transfected HBMVECs were seeded onto a confluent layer of fibroblasts, and lumen formation occurred by multicellular ECs at the sites of lateral EC-EC contacts and peaked between day 7-14 of co-culture. EC sprouts and lumens visualized by VE-cadherin and collagen IV staining were greatly enhanced by CCM3 deletion (**Fig.4a; Supplementary Fig.5a–b**). Quantitative analyses indicated that the number of branch points, mean lumen diameters and lumenized (collagen IV-covered) areas[37,38] in the CCM3-knockdown group were significantly increased (**Fig.4a–b**). Increased EC sprouting and enlarged lumen formation induced by CCM3 knockdown were not affected by control IgG treatment, but were blunted by either co-repression of UNC13B with its siRNA or by inhibition of ANGPT2 with the anti-ANGPT2 antibody (**Fig.4a–b**).

To further verify that CCM3 regulates EC lumen formation and PC recruitments, we performed a 3D spheroid sprouting assay in which ECs were coated onto cytodex beads following by embedding in fibrin gels. Fibroblasts cultured on top of the gel promoted optimal sprouting and tube formation which peaked at day 8 as visualized by immunostaining with VE-cadherin (**Supplementary Fig.5c–e**). Quantitative analyses indicated that the mean sprout length was not different between Ctrl and CCM3-knockdown groups, but the number of sprouts was drastically increased. Moreover, we detected dilated lumen formation in the CCM3-knockdown group (**Supplementary Fig.5c–f).** Importantly, increased EC sprouting and dilated lumen formation induced by CCM3 knockdown were blunted by either co-repression of UNC13B with siRNA or inhibition of ANGPT2 with anti-ANGPT2 antibody (Fig.4c–d).

The spheroid sprouting assay has been a system to study PC or smooth muscle cell recruitment and vessel maturation[39]. To visualize EC and PC in the sprouts, EGFP-expressing HBMVEC were transfected with a Ctrl or CCM3-siRNA followed by seeding with mCherry-expressing normal HBMVPC. PCs were recruited to Ctrl EC during sprouting, but CCM3 KD EC failed to recruit PCs (**Fig.4e**). However, co-repression of UNC13B in EC or addition of anti-ANGPT2 antibody or a combination of both in the sprouting assay restored PC recruitments to EC sprouts (**Fig.4e–f**). Our data suggest that CCM3 maintains normal EC junctions, EC lumen formation and PCs recruitment by restraining ANGPT2 exocytosis from EC.

Unc13b deficiency reduces ANGPT2 secretion and CCM lesions in *Ccm3*^{ECKO} mice

Unc13b$^{-/-}$ mice do not show gross phenotypes but develop seizures after one year of age, probably due to UNC13 function in the brains[40]. To test if suppression of the elevated exocytosis rescues CCM phenotypes in the mouse CCM models, *Ccm3*^{ECKO}:*Unc13b*$^{-/-}$ (DKO) mice were obtained by mating with *Unc13b*$^{-/-}$ mice with Cdh5-CreERT2:*Pdc10*$^{fl/fl}$ mice, followed by feeding pups with tamoxifen at P1 to P3. Brain tissues were harvested at P5 (early onset of the phenotypes) and P10 (full bloom of the lesion phenotypes). No lesions were found in the *Unc13b*$^{-/-}$ brain and the number of lesions (**Fig.5a–c**) and capillary dilation with defects in PC coverage induced by *Ccm3* deletion were significantly reduced in the cerebellar sections from the DKO mice (**Fig.5d–e**). Diffuse ANGPT2 staining surrounding dilated vessels with concomitant increases in phospho-TIE2 staining were detected in the *Ccm3*^{ECKO} mice as compared to the WT mice or *Unc13b*$^{-/-}$ mice. Phospho-TIE2-positive ECs increased in the diseased brains of the *Ccm3*^{ECKO} was much more subdued in the DKO mice (**Fig.5f–g**). Total ANGPT2 protein was weakly upregulated by Ccm3 but was restored by *Unc13b* deletion in brain tissues as measured by ELISA and Western blotting (**Fig.5h–i**). ANGPT2 secretion was significantly increased in isolated brain ECs from the diseased brains of the *Ccm3*^{ECKO} mice but was reduced by co-deletion of *Unc13b* (Fig.5j). These results strongly suggest that *Unc13b* deficiency, by suppressing the ANGPT2-TIE2 signaling in ECs, attenuates the neurovascular phenotypes caused by *Ccm3* inactivation.

ANGPT2 neutralization antibody blocks CCM lesion formation in *Ccm3*^{ECKO} mice

Anti-ANGPT2 antibody strongly inhibits angiogenesis at high doses[38,41]. When given i.p injection at 10 μg/g (body weight) from P2 and every other day thereafter, we observed weaker inhibitory effects of anti-ANGPT2 on retinal angiogenesis (~22%) and brain vascular density (~10%) (**Supplementary Fig.6**). CCM lesions in *Ccm3*^{ECKO} were drastically reduced by ANGPT2 neutralization antibody as visualized by whole-mount picture and H&E staining (**Fig.6a–c).** We further tested the combinatory effects of anti-ANGPT2 and *Unc13b* deficiency on CCM lesion development. Anti-ANGPT2 in DKO mice (*Ccm3*^{ECKO}:*Unc13b*$^{-/-}$) completely diminished CCM lesions. Similar results were obtained for the effects of anti-ANGPT2 antibody on CCM lesion development in the retinas (**Supplementary Fig.7a–c**). The NG2^{+} PC coverage of CD31^{+} microvessels was enhanced from 20% in IgG-treated *Ccm3*^{ECKO} mice to over 80% in anti-ANGPT2–treated *Ccm3*^{ECKO} mice and almost 100% in anti-ANGPT2 antibody-treated DKO mice (**Fig.6d–e**). Similar

results were observed for EC adherens junctions and tight junctions (**Fig.6d–e**). We determined the correlation of therapeutic effects of anti-ANGPT2 antibody with its effects on the ANGPT2-TIE2 signaling in vivo. Diffuse ANGPT2 staining surrounding dilated vessels with positive phospho-TIE2 staining were drastically increased in the *Ccm3*^{ECKO} mice (**Fig.6f,h**). ANGPT2 diffuse staining, total ANGPT2 protein and phospho-TIE2 were drastically reduced by anti-ANGPT2 antibody in *Ccm3*^{ECKO}, and completely abolished in the DKO mice (**Fig.6f-i**). Taken together, our data support the conclusion that CCM3 deletion induces ANGPT2 secretion from ECs, which disrupts EC junctions and EC-PC associations, and contributes to the CCM disease phenotypes.

DISCUSSION

In this study, we report that CCM lesions in the mice with an EC-specific *Ccm3* gene deletion (*Ccm3*^{ECKO}) exhibit cerebellum hemorrhage with disrupted EC junctions and EC-PC associations, correlating with increased ANGPT2 secretion surrounding the dilated cerebral microvessels. The enhanced ANGPT2 secretion is observed in brain and retina tissues, but not in the lung tissue or the blood of *Ccm3*^{ECKO} mice. A brain/retina-specific effect of CCM3 on ANGPT2 may provide a possible explanation for brain/retina-restrained CCM lesions in the EC-specific CCM3 deficient mice. In vitro studies confirm that CCM3 deficiency in ECs causes disruption of EC junctions, enlarged lumen formation and reduced PC recruitment during sprouting and tube formation. These EC phenotypes correlate with augmented ANGPT2 release and secretion from CCM3-ablated ECs, and are significantly attenuated by inhibition of exocytosis or neutralization of ANGPT2, suggesting that CCM3 maintains normal EC junctions, lumen formation and vessel maturation by restraining exocytosis-mediated ANGPT2 release from ECs. Mechanistic studies using confocal and TIRF microscopy analyses suggest that CCM3, by suppressing UNC13B/VAMP-dependent exocytosis, regulates ANGPT2 release from the Weibel-Palade bodies in brain ECs. Using mouse genetic approaches, we show that *Unc13b*-deficiency prevents disruption of the EC junctions and vessel dilation, and blocks CCM lesion development in the brains caused by EC-specific *Ccm3* inactivation. Importantly, our results demonstrate that an ANGPT2 neutralization antibody ameliorates CCM lesion progression in the mouse CCM models, correlating with normalized EC junction, EC-PC interaction and vascular integrity. Our study reveals a novel mechanism by which CCM3 mutations contribute to the progression of the CCM disease (**Supplemental Fig.8**), offering a therapeutic approach to this presently incurable pathology.

We have recently demonstrated that CCM3 in complex with GCKIII kinases binds to the C2B domain of UNC13 and inhibits its binding to plasma membrane lipids, a step required for exocytosis[24]. In the present study, we provide strong evidence that CCM3 through UNC13B/VAMP-dependent exocytosis controls ANGPT2 secretion in ECs. 1) We find that UNC13B is the primary isoform expressed in vascular ECs. Moreover, UNC13B forms a complex with CCM3 and GCKIII member STK24 in ECs. 2) By confocal analyses, CCM3 is co-localized with VAMP3 and VAMP8 in brain ECs. 3) By real-time TIRF microscopic analyses, we show that CCM3-depleted ECs increase exocytic fusion events; these increased fusion events can be suppressed by co-silencing of UNC13B. 4) Depletion of CCM3 (but not CCM1 or CCM2) in brain ECs strongly augments ANGPT2 secretion from the cells, which

could be blocked by co-silencing of UNC13B or VAMP3. However, ANGPT2 mRNA and total ANGPT2 protein are not dramatically altered by CCM3 deletion in ECs. Consistently, ANGPT2 protein stability and secretion are not altered in CCM3 depleted ECs, supporting that the primary mechanism for increases in ANGPT2 release by CCM3-deficiency is exocytosis rather than protein synthesis or protein stability. 5) By genetic approaches using *Ccm3*- and *Unc13b*-deficient mice, we observe similar regulatory patterns of ANGPT2 secretion by CCM3-UNC13B in mouse brain and retina tissues. 6) More importantly, we show that ANGPT2 neutralization antibody could normalize EC junctions and ameliorate CCM lesion progression in the mouse CCM models. Although *Angpt2*-deficient mice are viable[42], ANGPT2 is required for postnatal angiogenesis and lymphatic patterning[42]. ANGPT2 defects may cause glaucoma, a disease leading to blindness[43]. Clinically, an optimal dose of ANGPT2 may be necessary to achieve a maximum anti-CCM effect with minimum side effects on physiological vascular development and function.

TIE2 signaling pathway plays distinct roles in both vascular quiescence and angiogenesis. This has been attributed to distinct TIE2 signaling complexes assembled by ANGPT1 so that phosphor-TIE2 is located at EC-EC contacts in quiescent state but at EC-matrix contacts during angiogenesis[44,45]. Although ANGPT2 acts as a negative regulator of ANGPT1/TIE2 signaling in quiescent ECs, it is capable of inducing TIE2 phosphorylation in stressed ECs[38,46]. We observe increased ANGPT2-TIE2 signaling in CCM3-depleted ECs, consistent with the reports that CCM3 deletion induces several forms of stress-related signaling in ECs[47]. Our data indicate that increased ANGPT2 secretion in both CCM3-depleted brain tissues and brain ECs correlates with enhanced phospho-TIE2. It is plausible that ANGPT2 antagonizes ANGPT1 in quiescent ECs to inhibit TIE2 activation while it synergizes ANGPT1 in TIE2 phosphorylation to promote angiogenesis. Our data clearly demonstrated that enhanced ANGPT2-TIE2 signaling contributes to CCM pathogenesis. However, the pathological consequence of increased ANGPT2-TIE2 signaling from CCM3 loss might in fact be different from acute ANGPT2-TIE2 activation in acute inflammation because only CCM3 loss greatly increases EC lumen dilatation. It has been reported that loss of CCM1 or CCM2 in ECs activates several signaling pathways, including RhoA[48], the MEKK3–ERK5–Krüppel-like factor (KLF) 2/4 signaling[20,49], and the KLF4–TGF-β/Smad-mediated endothelial-mesenchymal transition (EndMT)[16,49]. It needs to be further defined if CCM3–UNC13–ANGPT2–TIE2 axis crosstalks with these pathways. Interestingly enough, ANGPT1/TIE2 via PI3K-Akt activation induces expression of KLF2 in quiescence ECs[50]. It is possible that in CCM3-depleted ECs ANGPT2 via TIE2 induces KLF2 expression, which serves a converging point of CCM3-mediated ANGPT2–TIE2 signaling and CCM1/2-mediated MEKK3–ERK5 signaling involved in CCM progression.

It is emerging that modulating EC junctions represents a common mechanism for all signaling pathways regulated by three CCM proteins, underlying potential mechanism in which mutations of any one of the three genes in human or deletion of any one of the three genes in postnatal mice results in similar CCM lesions. CCM1, in complex with CCM2, binds to and regulates several proteins directly involved in EC junctions and junction-associated complexes, such as Rap1, HEG (heart of glass) and ICAP-1 (integrin cytoplasmic domain associated protein-1)[51-53]. Our in vitro and in vivo data clearly demonstrate CCM3, by restraining ANGPT2 secretion, regulates both adherens and tight junctions in brain ECs.

It remains unknown exactly how alterations of EC junctions link with CCM lesion development. An important and common phenotype of CCM gene deletions is to cause enlarged lumen formation. It is known that EC junction organization directly regulates EC lumen formation[54]. In the early murine embryo, a homozygous null mutation of the gene encoding VE-cadherin (*Cdh5*) results in enlarged lumens of cephalic vessels although causing a reduction in lumenal size of the aorta and of cardinal veins[55,56]. Mechanistic studies suggest that CCM1-VE-cadherin directs association of adherens junction organization with the polarity complex to regulate vascular lumenal structure[54], and this could ne shared by CCM3. Alternatively, CCM3-mediated exocytosis may directly contribute to lumen formation. It is now accepted that lumen formation involves the structured expansion of the apical plasma membrane through general mechanism of vesicle transport[57]. This idea is supported by recent reports from fly genetic studies of tracheal tubule formation. The loss-of-function mutants of fly CCM3 or GCKIII kinase ortholog have dilated tracheal tubes, which resemble dilated blood vessels found in CCM patients[58]. This tube dilation phenotype can be suppressed by the reduction in the expression of NSF2, a protein involved in SNARE recycling and the secondary phase of exocytosis. It is known that CCM lesions have a predilection for the vessels of the brain and retinas, which are unique in having an extraordinarily high PC to EC ratio, forming a high resistance blood-brain barrier or blood-retinal barrier further supplemented by astrocyte foot processes. Our in vitro model study indicates that loss of CCM3 in ECs causes dilated lumen with impaired PC recruitment, recapitulating CCM lesion phenotype in vivo. Moreover, ANGPT2 plays a critical role in modulating CCM3-mediated EC-PC interactions. Therefore, identification of ANGPT2 as a CCM3 (but not CCM1 or CCM2) downstream effector may explain why CCM3 mutations in human often result in a more severe form of the disease.

ONLINE METHODS

Generation of tamoxifen-inducible endothelial-specific *Ccm3* deficient mice (*Ccm3*^{ECKO})

Tomato reporter mice were purchased from The Jackson Laboratory (Stock No.007576; strain name STOCK Gt (ROSA)26Sor$^{tm4(ACTB-tdTomato,-EGFP)Luo}$/J). *Pdc10*$^{fl/fl}$ mice were crossed with *Cdh*5-CreERT2 mice in which the Cre recombinase expression is driven by the *Cdh*5 promoter to generate mice with inducible endothelial cell (EC)-specific deletion of *Pdcd10* (designated *Ccm3*^{ECKO}). For the *in vivo* tamoxifen-induced *Ccm3* deletion, tamoxifen (Sigma, T5648) was diluted at 10 mg/ml and fed 10 μg/g (body weight) once daily from postnatal day (P)1 to P3 in *Ccm3*^{ECKO} and WT control mice *(Pdcd10*$^{fl/fl}$) newborn pups. *Unc13B*-deficient mice do not show gross phenotypes but develop seizures after one year of age, probably due to loss of UNC13 function in the brains. Mice were cared for in accordance with National Institutes of Health guidelines, and all procedures were approved by the Yale University Animal Care and Use Committee.

Clinical specimens

Ethical evaluation for the clinical specimens was reviewed and approved by the Yale human Investigation Committee (IHC# 0601000969). The Section of Neuropathology, Department of Pathology at Yale University School of Medicine archives human specimens including CCM3 samples from consenting patients or family members. All of the samples were

independently evaluated by two pathologists, who were experienced in evaluating immunohistochemistry and had no prior information regarding the clinical outcome of the patients. We obtained paraffin blocks for 8 cases of CCM3 lesions and each block was cut into 20 more slides. We found 6 samples contained typical CCM lesions with normal surrounding tissues based on H&E staining, and these were used further for immunostaining. Two cases showed severe vascular fibrosis and were not used for further analyses (**Supplementary Fig.3**).

Treatment with ANGPT2 neutralizing antibody in vivo

Humanized mouse monoclonal ANGPT2 neutralizing antibody (Genentech Inc. or Darron Medscience, Co.) was dissolved in sterile PBS at 1 mg/ml. ANGPT2 neutralizing antibody or control IgG1 were intraperitoneally injected (10 μg/g body weight) to littermate of WT or to *Ccm3*^{ECKO} pups from P2 and every other day thereafter.

FITC-dextran perfusion and Evan Blue Dye (EBD) permeability assays

FITC-dextran (FD2000S; Sigma-Aldrich, St. Louis, MO, USA) was dissolved in sterile normal saline at a concentration of 50 mg/ml followed by centrifugation at 10,000 x g for 5 min. The supernatant was collected and protected from light for injection. Littermate of WT or *Ccm3*^{ECKO} pups with or without anti-ANGPT2 treatment were weighed and anesthetized with an intraperitoneal (IP) injection of anesthetic (katamine 100 mg/kg + xylazine 10mg/kg). The retro-orbital injection was followed by the published protocols. Briefly, the lateral canthus of the left orbit was chosen as the injection site. A 31-gauge needle with a 3/10 ml insulin syringe was used to gently pierce into the mouse's orbital venous sinus about 2-3 mm with the bevel of the needle facing upward at a 45° angle. 10 μl per g body weight of FITC-dextran was injected into each pup and waited for 5 min. Brains and retinas were harvested and fixed for sectional or whole mount fluorescent immunostaining.

EBD permeability assay (Miles assay) was performed. Briefly, Evans Blue Dye (100 μl of a 1% solution in 0.9% NaCl; Sigma-Aldrich) was injected into the retro-orbital plexus of anesthetized WT and *Ccm3*^{ECKO} mice. 30 minutes after the injection, mice were sacrificed and perfused with PBS through the left ventricle to clear the dye from the vascular volume. Cerebellum tissues were harvested and dried in 60°C overnight, and weighed before Evans blue extraction using 1 ml formamide at 55°C for 16 h. Evans blue content was quantified by reading at 630 nm in a spectrophotometer.

Immunofluorescence analysis

Mouse brains were harvested, fixed with 4% PFA, embedded in OCT and sectioned (5 μm thick). Slides were washed with PBS twice to remove OCT, and 5% donkey serum in 0.3% TritonX-100 in PBS was used for half hour to block non-specific staining and to permeabilize section tissue. Slides were incubated with primary antibodies such as anti-CD31 (1:100), anti-NG2 (1:100), anti-VE-cadherin (1:100), anti-ZO-1 (1:100), anti-Claudin-5 (1:100), anti-Angiopoietin-2 (1:100), and anti-Connexin-43 (1:100) overnight at 4?,then were washed with PBS three times and incubated with secondary antibodies (1:200 to 1:400) at room temperature for one hour. After washed in PBS three more times, slides were mounted with VECTASHIELD Mounting medium with DAPI (Vector Laboratory),

and photographed. HBMVECs were fixed in 4% PFA for 20 mins, washed with PBS and permeabilized with 0.1% Triton X-100 for 2 mins. After half hour blocking, primary and secondary antibodies were applied sequentially. Mounting and photographing methods were the same as tissue staining.

Fluorescent staining of whole-mount retinas

FITC-dextran perfused eyes from neonatal mice were collected on P5-P15 and fixed in 4% paraformaldehyde for 2 hours on ice. For dissection, the cornea, lens, sclera and hyaloid vessels were removed. Retinas were permeabilized in 0.5%Triton/PBS (5% normal donkey serum) overnight at 4°C, followed by incubation with primary antibodies diluted 1:50 in 0.1% Triton/PBS (1% normal donkey serum) overnight at 4°C and then incubated with fluorescent second antibody overnight at 4°C after wash. Retinas were then washed 5 times with PBS and mounted by making four incisions in fluorescent mounting medium. Pictures were taken with the same exposure and gain using a confocal Leica TCS CP5 microscope (Leica, Germany). Vascular areas were outlined using NIH Image J software and quantified as the percentage of total area of retina analyzed.

Gene expression in the tissues

Total RNAs were isolated from tissues by using the RNeasy kit with DNase I digestion (Qiagen, Valencia, CA). Reverse transcription (RT) was done by standard procedure (Super Script first-strand synthesis system; Qiagen) using 1 μg total RNA. Quantitative real-time polymerase chain reaction (qPCR) was performed by using iQ SYBR Green Supermix on iCycler real-time detection system (Bio-Rad Laboratories, Inc., Hercules, CA). qRT-PCR with specific primers (e.g., ANGPT1, ANGPT2 and Tie-2) were performed.

Cell Culture and growth factors

Mouse brain microvascular ECs (MBMVECs) were isolated as we described previously[32]. Purity of ECs was verified by cell morphology, positive staining for VE-cadherin, von Willebrand factor, CD31 and VEGFR2 signaling, but negative for PCs markers (SMA and NG2). Primary ECs used for experiments were at passages three or less. CCM3 deletion in mouse EC was achieved by treatment with 4-hydroxyl tamoxifen (Sigma, H7904) at 100 nM and mock (DMSO/Ethanol)-treated cells were used as control. Human brain microvascular ECs (HBMVECs; cAP0002) and brain microvascular PCs (HBMVPCs; cAP-0030) were purchased from Angio-Proteomie (Boston). ECs were grown in Microvascular Endothelial Cell Growth Medium-2 MV (EGM2, Lonza) and HBMVPCs were grown in pericyte growth medium containing FBS and growth factor supplement (Angio-Proteomie). Human lung fibroblasts were routinely grown in DMEM supplemented with 10% FBS at 37°C and 5% CO_2 and used between passages 10 to 14.

Lentiviral vector and packaging system

The Trans-Lentiviral Packaging System was used. The coding sequences for CCM3-WT (1-212aa) and CCM3-N (a truncated mutant containing the N-terminal 1-95aa that was found in human patients) were cloned into pLEX MCS vector (Clontech). Lentivirus expressing mCherry (rLV.EF1.mCherry-9) was purchased from Clontech. Plasmids were

transfected and lentiruses were packed. Briefly, conditioned medium was harvested 62 hours after transfection, cleared of debris by low-speed centrifugation, filtered through 0.45-μM filters (Falcon, Lincoln Park, NJ), and assayed for transduction of HBMVEC, by infecting cells overnight with serial dilutions of vector stock in culture medium supplemented with 8 μg/ml Polybrene (Sigma, St. Louis, MO). After medium replacement, the cells were further incubated for 36 hours, and expression of RFP was scored by microscopy. The CCM3 mutants expression was determined by western blot. Concentrated vector stocks were prepared by ultracentrifugation of conditioned medium at 50,000*g* for 90 minutes. The pellet was resuspended in 0.05% of the starting volume in sterile PBS containing 4 μg/ml Polybrene. Stocks were titered as described above and stored frozen at −80°C.

ANGPT2 ELISA

For measurement of ANGPT2 in human EC supernatant, the cells were treated and harvested at indicated times. ELISA was performed with standard sandwich ELISA assay using anti-ANGPT2 antibodies from R&D, recombinant human ANGPT2 (625-AN-025), human ANGPT2 Mab (MAB098), human ANGPT2 biotinylated Mab (Bam0981). For measurement of ANGPT2 in mouse cells and tissues, the Angpt2 mouse ELISA kits were from R&D (MANG20) and ABCAM (ab171335). For Western blotting, mouse tissues were snap-frozen and tissues were homogenized in RIPA lysis buffer prior to SDS-PAGE. For ELISA assay, fresh mouse tissues were minced followed by incubation in serum-free medium for 2 h. ANGPT2 proteins in Supernatants were measured.

Real-time TIRF microscopy

TIRF imaging was performed using an IX-70 inverted microscope (Olympus), equipped with an argon (488 nm) laser line, a custom TIRFM condenser, a 60 × 1.45 NA TIRF objective (Olympus), and an EMCCD camera (iXon887; Andor Technology). Imaging system was controlled using the iQ software (Andor Technology). For live-cell image, HBMVEC cells were seeded into 35 mm petri dishes with a No. 1.5 coverglass at the bottom (MatTek, Ashland, MA) in the EGM-2-MV culture medium (Lonza, cc-3202). They were first transfected with siRNAs using RNAiMAX (ThermoFisher). After 24 hours, the cells were transfected with the VAMP8-PHluorin plasmid using the Cytofect-Endothelial transfection kit (Cell Applications Inc., TF101K). After another 24 hours, time-lapsed images of the transfected cells were acquired at 200 millisecond intervals at 37°C in a custom incubation chamber. Stacks of time-lapse images were processed and analyzed using a algorithm within Image J 1.42 (National Institutes of Health) by a custom-written MATLAB program.

Transendothelial Flux and TEER Measurements

For transendothelial flux measurements, ECs were seeded onto fibronectin-coated 96W20idf gold electrode ECIS cultureware (Applied BioPhysics) in the EGM-2 medium (Lonza, cc-3202) and then transfected with siRNAs. Barrier function of ECs was assessed by electrical cell-substrate impedance sensing (Applied BioPhysics) for 72 hours.

Organotypic angiogenesis assay

We employed a modified protocol for organotypic angiogenesis[37]. 8.5 ×10^3 HBMVECs with or without EGFP expression (infected by retrovirus; MOI 20) were transfected with siRNAs followed by seeding onto confluent human fibroblasts that had been plated at 2 × 10^4 cells onto 24-well plates and grown to confluency over 7–14 days. Seeding was 48 h after EC infection or 24 h after transfection in EGM2, which was replenished every 2 days. Tubule formation was assessed 2–14 days after seeding by VE-cadherin and collagen IV staining or by visualization of EGFP-expressing EC grown on glass bottom dishes (Mat Tek Corporation).

Three-dimensional bead sprouting assay

MBMVECs were transfected with siCtrl, siUNC13, siCCM3 or siCCM3 and siUNC13B overnight by Lipofectamine RNAiMAX following protocols provided by the manufacturer (Invitrogen) and changed to fresh prepared Microvascular Endothelial Cell Growth Medium-2 MV (EGM2, Lonza). Three-dimensional bead sprouting assay was performed according to a published protocol [36]. Briefly, cells were harvested at 24 hours post-transfection and were coated with Cytodex 3 microcarrier beads (C3275, Sigma) with a concentration of 400 cells per bead in EGM2 medium. These coated beads were embedded in 2 mg/ml fibrin gels in 24-well plates by mixing 2 mg/ml fibrinogen (Calbiochem) in DPBS, 0.625 U/mL thrombin (Sigma-Aldrich), and 0.15 Units/ml aprotinin (Sigma-Aldrich). EGM2 medium containing fibroblasts (20,000 per well) was added to each well with or without ANGPT2 neutralizing antibody (1 μg/ml or 10 μg/ml; Genentech). The cultures were maintained for 2–13 days by changing the medium every other day. Bright field images were captured with Axiovert 200 (Zeiss) at 10× magnification and sprout lengths were measured with NIH Image J.

HBMVECs and HBMVPCs co-culture system in three-dimensional bead sprouting assay

The spheroid sprouting assay for EC-PC interaction was performed. HBMVECs were infected with EGFP-expressing retrovirus and HBMVPCs were infected with mCherry-expressing lentiviruses (MOI 20). ECs were further transfected with siRNAs as indicated. ECs and PCs (2:1) were seeded to Cytodex 3 microcarrier beads (Sigma) with the concentration of 400 cells per bead in Microvascular Endothelial Cell Growth Medium-2 MV (EGM2, Lonza). We chose a 2:1 ratio based on our results showing that PCs grew faster than ECs and limited EC sprouting when at a 1:1 ratio. These coated beads were embedded in fibrin gels as shown above. EGM2 medium containing fibroblasts (20,000 per well) was added to each well with or without ANGPT2 neutralizing antibody (1 μg/ml or 10 μg/ml; Genentech). The cultures were maintained for 8 days by changing the medium every other day. Fluorescence images were captured with Axiovert 200 (Zeiss) at 10× magnification and the percentages of pericyte coverage of EC tubes were measured with NIH Image J.

Study Design and Statistical Analysis

Group sizes were determined by an *a priori* power analysis for a two-tailed, two-sample *t*-test with an α of 0.05 and power of 0.8, in order to detect a 10% difference in lesion size at the endpoint. Animal were grouped with no blinding but randomized during the

experiments. Male and female animals were used in equal numbers for all experiments. No samples or animals were excluded from analysis. All quantifications (lesion sizes, junctional integrity, sprout length and lumen) were performed in a blind fashion. All figures are representative of at least three experiments unless otherwise noted. All graphs report mean ± s.e.m values of biological replicates. Comparisons between two groups were performed by unpaired, two tailed t-test, between more than two groups by one-way ANOVA followed by Bonferroni's post-hoc or by two-way ANOVA using Prism 6.0 software (GraphPad). P values were two-tailed and values < 0.05 were considered to indicate statistical significance. $P < 0.05$, $P < 0.01$ and $P < 0.001$ are designated in all figures with *, **, ***, respectively.

List of Antibodies

The following antibodies were used for immunostaining:

Antibody name	Company	Cat#	Dilution
Angiopoietin-1, goat	Abcam	ab133425	1:200
Angiopoietin-2, goat	R&D	AF623	1:100
Angiopoietin-2, rabbit	Abcam	ab8452	1:200
Angiopoietin-2, rabbit	Novus	NBP2-1538	1:100
Beta-Catenin, mouse	BD Pharmingen	51-9001921	1:100
CCM3, mouse	Santa Cruz	SC365587	1:1000
CCM3, rabbit	Min lab		1:1000
CD31, rat	BD Pharmingen	553370	1:100
CD31, rabbit	Abcam	ab28364	1:100
Claudin-5, rabbit	Invitrogen	34-1600	1:100
Collagen IV, rabbit	AbD Serotec	2150-1470	1:300
Collagen IV, rabbit	Abcam	ab6586	1:500
Connexin-43, mouse	BD Pharmingen	51-9001918	1:100
NG2, rabbit	Millipore	AB5320	1:100
Phospho-TIE2 (Tyr992), rabbit	Cell Signaling	4226	1:1000
Phospho-Tie2 (Y992), rabbit	R&D	AF2720	1:100
TIE2, rabbit	Cell Signaling	4224	1:1000
VAMP3, goat	Santa Cruz	Sc-18208	1:100
VE-cadherin, rat	BD Pharmingen	555289	1:100
VE-cadherin, goat	Santa Cruz	sc-6458	1:100
ZO-1, rabbit	Invitrogen	61-7300	1:100
Alexa Flour 488 Phalloidin	Invitrogen	A12379	1:1000
Alexa Flour 594 Isolectin GS-IB4 conjugate	Invitrogen	I21413	1:50
Alexa Flour 488 Donkey Anti-Rat IgG	Invitrogen	A21208	1:200
Alexa Flour 488 Donkey Anti-Goat IgG	Invitrogen	A11055	1:200
Alexa Flour 488 Donkey Anti-Rabbit IgG	Invitrogen	A21206	1:200
Alexa Flour 488 Donkey Anti-Mouse IgG	Invitrogen	A21202	1:200
Alexa Flour 594 Donkey Anti-Rat IgG	Invitrogen	A21209	1:200
Alexa Flour 594 Donkey Anti-Goat IgG	Invitrogen	A11058	1:200
Alexa Flour 594 Donkey Anti-Rabbit IgG	Invitrogen	A21207	1:200

The following antibodies were used for immunostaining:			
Antibody name	**Company**	**Cat#**	**Dilution**
Alexa Flour 594 Donkey Anti-Mouse IgG	Invitrogen	A21203	1:200

The following antibodies were used for Western blot:

Rabbit polyclonal antibody against CCM3 was generated (Invitrogen) against full-length recombinant human CCM3 protein expressed and purified from Escherichia coli. Beta-Actin is from Sigma (mouse, A1978); GAPDH (rabbit, 2118), p-Smad2 (rabbit, 3180), p-MLC (rabbit, 3674), VEGFR2 (rabbit, 2479), p-TIE2 (rabbit, 4221), TIE2 (rabbit, 4224), p-FAK (rabbit, 3281) are from Cell Signaling Technology; Beta-Catenin (mouse, sc-7963), Cdc42 (mouse, sc-8401), Rac1 (sc-217), RhoA (mouse, sc-418), STK25 (goat, sc-6865) and VAMP-3 (goat, sc-18208) are from Santa Cruz Biotechnology. ANGPT2 (rabbit, Ab8452) is from Abcam and ANGPT2 (AF7186) from R&D; Integrin beta-1 (mouse, 610467) and FAK (mouse, 610087) are from BD. All first antibodies were used at 1:1000 dilution.

The uncropped gel images for Western blotting are presented at **Supplementary Data Set 1**.

Supplementary Material

Refer to Web version on PubMed Central for supplementary material.

ACKNOWLEDGEMENTS

Unc13B-deficient mice were a gift from Dr. Nils Brose (Max Planck Institute of Experimental Medicine, Germany). We thank Drs. J. Pober, R. Liu, and T. Manes for reagents and discussion. This work was partly supported by NIH grants R01 HL109420 WM), HL115148 (WM), GM109487 (DW), National Natural Science Foundation of China (No. 91539110) (WM), Scientific Grants of Guangdong (No. 2015B020225002 and 2015A050502018) (WM), American Hear Association grant 13SDG17110045 (HZ) and 14SDG20490020 (WT).

Abbreviations

ANGPT2	angiopoietin-2
CCM	Cerebral cavernous malformation
DAPI	4′,6-diamidino-2-phenylindole
EC	endothelial cell
EndMT	endothelial-mesenchymal transition
FITC-Dextran	fluorescein isothiocyanate-dextran
HBMVEC	human brain microvascular ECs
HBMVPC	human brain microvascular pericytes
KD	knockdown
KO	knockout
KLF2	Krüppel-like factor 2
MBMVEC	Mouse brain microvascular ECs
NSF	soluble *N*-ethylmaleimide–sensitive factor
SNARE	NSF attachment protein receptor (SNARE)

PC	pericyte
siRNA	small interfering RNA
TIRF	Total internal reflection fluorescence
VAMPs	vesicle-associated membrane proteins

REFERENCES

1. Revencu N, Vikkula M. Cerebral cavernous malformation: new molecular and clinical insights. J Med Genet. 2006; 43:716–721. [PubMed: 16571644]
2. Cavalcanti DD, et al. Cerebral cavernous malformations: from genes to proteins to disease. J Neurosurg. 2012; 116:122–132. [PubMed: 21962164]
3. Tanriover G, et al. Ultrastructural analysis of vascular features in cerebral cavernous malformations. Clinical neurology and neurosurgery. 2013; 115:438–444. [PubMed: 22776801]
4. Riant F, Bergametti F, Ayrignac X, Boulday G, Tournier-Lasserve E. Recent insights into cerebral cavernous malformations: the molecular genetics of CCM. FEBS J. 2010; 277:1070–1075. [PubMed: 20096038]
5. Labauge P, Denier C, Bergametti F, Tournier-Lasserve E. Genetics of cavernous angiomas. Lancet Neurol. 2007; 6:237–244. [PubMed: 17303530]
6. Sahoo T, et al. Mutations in the gene encoding KRIT1, a Krev-1/rap1a binding protein, cause cerebral cavernous malformations (CCM1). Hum Mol Genet. 1999; 8:2325–2333. [PubMed: 10545614]
7. Liquori CL, et al. Mutations in a gene encoding a novel protein containing a phosphotyrosine-binding domain cause type 2 cerebral cavernous malformations. Am J Hum Genet. 2003; 73:1459–1464. [PubMed: 14624391]
8. Bergametti F, et al. Mutations within the programmed cell death 10 gene cause cerebral cavernous malformations. Am J Hum Genet. 2005; 76:42–51. [PubMed: 15543491]
9. Gault J, Shenkar R, Recksiek P, Awad IA. Biallelic somatic and germ line CCM1 truncating mutations in a cerebral cavernous malformation lesion. Stroke. 2005; 36:872–874. [PubMed: 15718512]
10. Akers AL, Johnson E, Steinberg GK, Zabramski JM, Marchuk DA. Biallelic somatic and germline mutations in cerebral cavernous malformations (CCMs): evidence for a two-hit mechanism of CCM pathogenesis. Hum Mol Genet. 2009; 18:919–930. [PubMed: 19088123]
11. Pagenstecher A, Stahl S, Sure U, Felbor U. A two-hit mechanism causes cerebral cavernous malformations: complete inactivation of CCM1, CCM2 or CCM3 in affected endothelial cells. Hum Mol Genet. 2009; 18:911–918. [PubMed: 19088124]
12. McDonald DA, et al. A novel mouse model of cerebral cavernous malformations based on the two-hit mutation hypothesis recapitulates the human disease. Hum Mol Genet. 2011; 20:211–222. [PubMed: 20940147]
13. Chan AC, et al. Mutations in 2 distinct genetic pathways result in cerebral cavernous malformations in mice. J Clin Invest. 2011; 121:1871–1881. [PubMed: 21490399]
14. Cunningham K, et al. Conditional deletion of Ccm2 causes hemorrhage in the adult brain: a mouse model of human cerebral cavernous malformations. Hum Mol Genet. 2011; 20:3198–3206. [PubMed: 21596842]
15. Boulday G, et al. Tissue-specific conditional CCM2 knockout mice establish the essential role of endothelial CCM2 in angiogenesis: implications for human cerebral cavernous malformations. Dis Model Mech. 2009; 2:168–177. [PubMed: 19259391]
16. Maddaluno L, et al. EndMT contributes to the onset and progression of cerebral cavernous malformations. Nature. 2013; 498:492–496. [PubMed: 23748444]
17. Shenkar R, et al. Exceptional aggressiveness of cerebral cavernous malformation disease associated with PDCD10 mutations. Genetics in medicine : official journal of the American College of Medical Genetics. 2014

18. Whitehead KJ, et al. The cerebral cavernous malformation signaling pathway promotes vascular integrity via Rho GTPases. Nat Med. 2009; 15:177–184. [PubMed: 19151728]
19. Stockton RA, Shenkar R, Awad IA, Ginsberg MH. Cerebral cavernous malformations proteins inhibit Rho kinase to stabilize vascular integrity. J Exp Med. 2010; 207:881–896. [PubMed: 20308363]
20. Zhou Z, et al. Cerebral cavernous malformations arise from endothelial gain of MEKK3-KLF2/4 signalling. Nature. 2016
21. Denier C, et al. Genotype-phenotype correlations in cerebral cavernous malformations patients. Ann Neurol. 2006; 60:550–556. [PubMed: 17041941]
22. Zheng X, et al. CCM3 signaling through sterile 20-like kinases plays an essential role during zebrafish cardiovascular development and cerebral cavernous malformations. J Clin Invest. 2010; 120:2795–2804. [PubMed: 20592472]
23. Yoruk B, Gillers BS, Chi NC, Scott IC. Ccm3 functions in a manner distinct from Ccm1 and Ccm2 in a zebrafish model of CCM vascular disease. Dev Biol. 2012; 362:121–131. [PubMed: 22182521]
24. Zhang Y, et al. A network of interactions enables CCM3 and STK24 to coordinate UNC13D-driven vesicle exocytosis in neutrophils. Dev Cell. 2013; 27:215–226. [PubMed: 24176643]
25. Feldmann J, et al. Munc13-4 is essential for cytolytic granules fusion and is mutated in a form of familial hemophagocytic lymphohistiocytosis (FHL3). Cell. 2003; 115:461–473. [PubMed: 14622600]
26. Jahn R, Sudhof TC. Membrane fusion and exocytosis. Annu Rev Biochem. 1999; 68:863–911. [PubMed: 10872468]
27. Lowenstein CJ, Morrell CN, Yamakuchi M. Regulation of Weibel-Palade body exocytosis. Trends Cardiovasc Med. 2005; 15:302–308. [PubMed: 16297768]
28. Fiedler U, et al. Angiopoietin-2 sensitizes endothelial cells to TNF-alpha and has a crucial role in the induction of inflammation. Nat Med. 2006; 12:235–239. [PubMed: 16462802]
29. Gaengel K, Genove G, Armulik A, Betsholtz C. Endothelial-mural cell signaling in vascular development and angiogenesis. Arterioscler Thromb Vasc Biol. 2009; 29:630–638. [PubMed: 19164813]
30. Eklund L, Olsen BR. Tie receptors and their angiopoietin ligands are context-dependent regulators of vascular remodeling. Exp Cell Res. 2006; 312:630–641. [PubMed: 16225862]
31. Maisonpierre PC, et al. Angiopoietin-2, a natural antagonist for Tie2 that disrupts in vivo angiogenesis. Science. 1997; 277:55–60. [PubMed: 9204896]
32. He Y, et al. Stabilization of VEGFR2 signaling by cerebral cavernous malformation 3 is critical for vascular development. Sci Signal. 2010; 3:ra26. [PubMed: 20371769]
33. Fidalgo M, et al. CCM3/PDCD10 stabilizes GCKIII proteins to promote Golgi assembly and cell orientation. J Cell Sci. 2010; 123:1274–1284. [PubMed: 20332113]
34. Zhou HJ, et al. AIP1 Mediates Vascular Endothelial Cell Growth Factor Receptor-3-Dependent Angiogenic and Lymphangiogenic Responses. Arterioscler Thromb Vasc Biol. 2014; 34:603–615. [PubMed: 24407031]
35. Kluger MS, Clark PR, Tellides G, Gerke V, Pober JS. Claudin-5 controls intercellular barriers of human dermal microvascular but not human umbilical vein endothelial cells. Arterioscler Thromb Vasc Biol. 2013; 33:489–500. [PubMed: 23288152]
36. Nakatsu MN, Hughes CC. An optimized three-dimensional in vitro model for the analysis of angiogenesis. Methods Enzymol. 2008; 443:65–82. [PubMed: 18772011]
37. Abraham S, et al. A Rac/Cdc42 exchange factor complex promotes formation of lateral filopodia and blood vessel lumen morphogenesis. Nature communications. 2015; 6:7286.
38. Felcht M, et al. Angiopoietin-2 differentially regulates angiogenesis through TIE2 and integrin signaling. J Clin Invest. 2012; 122:1991–2005. [PubMed: 22585576]
39. Chang WG, Andrejecsk JW, Kluger MS, Saltzman WM, Pober JS. Pericytes modulate endothelial sprouting. Cardiovasc Res. 2013; 100:492–500. [PubMed: 24042014]

40. Varoqueaux F, et al. Total arrest of spontaneous and evoked synaptic transmission but normal synaptogenesis in the absence of Munc13-mediated vesicle priming. Proc Natl Acad Sci U S A. 2002; 99:9037–9042. [PubMed: 12070347]
41. Holopainen T, et al. Effects of angiopoietin-2-blocking antibody on endothelial cell-cell junctions and lung metastasis. J Natl Cancer Inst. 2012; 104:461–475. [PubMed: 22343031]
42. Gale NW, et al. Angiopoietin-2 is required for postnatal angiogenesis and lymphatic patterning, and only the latter role is rescued by Angiopoietin-1. Dev Cell. 2002; 3:411–423. [PubMed: 12361603]
43. Thomson BR, et al. A lymphatic defect causes ocular hypertension and glaucoma in mice. J Clin Invest. 2014; 124:4320–4324. [PubMed: 25202984]
44. Saharinen P, et al. Angiopoietins assemble distinct Tie2 signalling complexes in endothelial cell-cell and cell-matrix contacts. Nat Cell Biol. 2008; 10:527–537. [PubMed: 18425119]
45. Fukuhara S, et al. Differential function of Tie2 at cell-cell contacts and cell-substratum contacts regulated by angiopoietin-1. Nat Cell Biol. 2008; 10:513–526. [PubMed: 18425120]
46. Daly C, et al. Angiopoietin-2 functions as an autocrine protective factor in stressed endothelial cells. Proc Natl Acad Sci U S A. 2006; 103:15491–15496. [PubMed: 17030814]
47. Marchi S, et al. Defective autophagy is a key feature of cerebral cavernous malformations. EMBO Mol Med. 2015; 7:1403–1417. [PubMed: 26417067]
48. Gingras AR, Liu JJ, Ginsberg MH. Structural basis of the junctional anchorage of the cerebral cavernous malformations complex. J Cell Biol. 2012; 199:39–48. [PubMed: 23007647]
49. Cuttano R, et al. KLF4 is a key determinant in the development and progression of cerebral cavernous malformations. EMBO Mol Med. 2015; 8:6–24. [PubMed: 26612856]
50. Sako K, et al. Angiopoietin-1 induces Kruppel-like factor 2 expression through a phosphoinositide 3-kinase/AKT-dependent activation of myocyte enhancer factor 2. J Biol Chem. 2009; 284:5592–5601. [PubMed: 19106103]
51. Zawistowski JS, et al. CCM1 and CCM2 protein interactions in cell signaling: implications for cerebral cavernous malformations pathogenesis. Hum Mol Genet. 2005; 14:2521–2531. [PubMed: 16037064]
52. Pouwels J, Nevo J, Pellinen T, Ylanne J, Ivaska J. Negative regulators of integrin activity. J Cell Sci. 2012; 125:3271–3280. [PubMed: 22822081]
53. Brutsch R, et al. Integrin cytoplasmic domain-associated protein-1 attenuates sprouting angiogenesis. Circ Res. 2010; 107:592–601. [PubMed: 20616313]
54. Lampugnani MG, et al. CCM1 regulates vascular-lumen organization by inducing endothelial polarity. J Cell Sci. 2010; 123:1073–1080. [PubMed: 20332120]
55. Carmeliet P, et al. Targeted deficiency or cytosolic truncation of the VE-cadherin gene in mice impairs VEGF-mediated endothelial survival and angiogenesis. Cell. 1999; 98:147–157. [PubMed: 10428027]
56. Gory-Faure S, et al. Role of vascular endothelial-cadherin in vascular morphogenesis. Development. 1999; 126:2093–2102. [PubMed: 10207135]
57. Sigurbjornsdottir S, Mathew R, Leptin M. Molecular mechanisms of de novo lumen formation. Nat Rev Mol Cell Biol. 2014; 15:665–676. [PubMed: 25186133]
58. Song Y, Eng M, Ghabrial AS. Focal defects in single-celled tubes mutant for Cerebral cavernous malformation 3, GCKIII, or NSF2. Dev Cell. 2013; 25:507–519. [PubMed: 23763949]

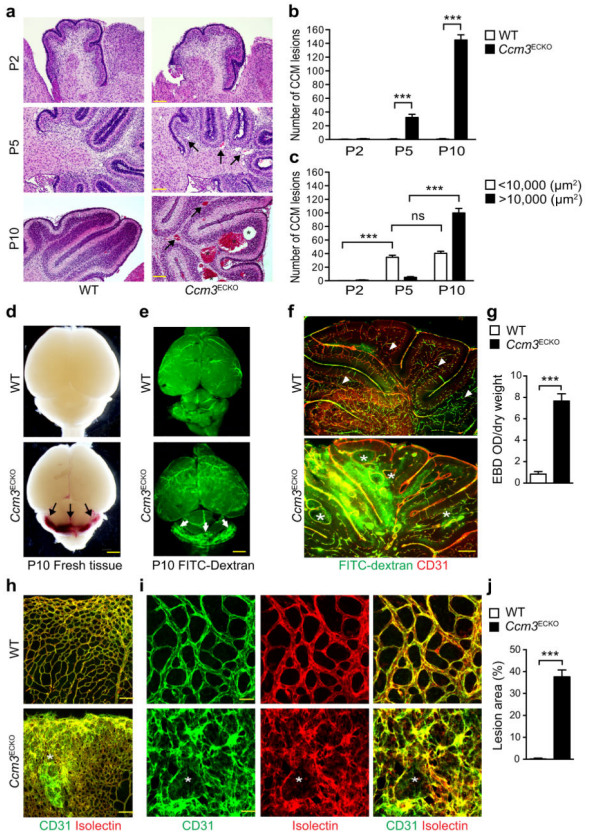

Fig.1. EC-inducible *Ccm3* deletion (*Ccm3*^{ECKO}) mice develop CCM lesions

a–c. CCM lesion quantification in WT (*Pdcd10*$^{fl/fl}$) and *Ccm3*^{ECKO} (Cdh5CerERT2;*Pdcd10*$^{fl/fl}$). (**a**) H&E staining of cerebellum sections. Representative images of small lesions (arrows) and large lesions (asterisks) are shown. Number of total lesions (**b**) and lesions with different sizes (**c**) in *Ccm3*^{ECKO} mice were quantified (n=10). ns: non-significant; **P<0.01; ***P<0.001 (two-way ANOVA). **d–g**. Vascular leakage in CCM lesions. (**d**) Images for fresh brain tissue of WT and *Ccm3*^{ECKO} mice at P10. (**e–f**) P10 pups were perfused with FITC-dextran (2000 kDa) and brain sections were subjected to immunostaining with anti-CD31. Vascular leakage is indicated by arrows in panel **e**. CCM lesions are indicated by asterisks whereas arrowheads indicate a normal granule cell layer within each lobule of cerebella in WT mice (**f**). (**g**) Cerebellum permeability was measured by Evan's blue dye (EBD) assay in WT and *Ccm3*^{ECKO} mice (n=10). **P<0.01 (unpaired two-tailed Student's t-test). **h–j.** Lesions in retinas. P10 retinas from WT and *Ccm3*^{ECKO} pups were stained with EC markers CD31 (green) and isolectin B4 (red). CCM lesions with disorganized vasculatures are indicated by asterisks in confocal images of **h** (20×) and **i** (80×). Lesion areas (% of total retina) are quantified by Image J (**j**). n=10, **P<0.01 (unpaired two-tailed Student's t-test). Error bars indicate s.e.m. Scale bars: **a**: 400 μm; **f**, **h**: 100 μm; **d–e**: 2 mm; **i**: 25 μm.

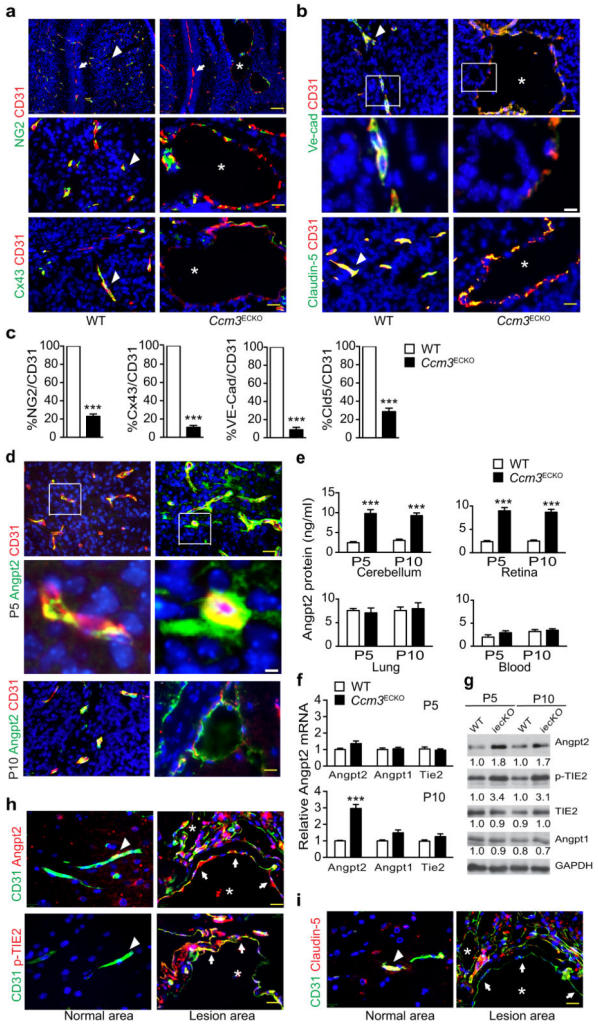

Fig.2. *Ccm3*$^{\text{ECKO}}$ mice exhibit disrupted EC-PC and EC-EC junctions with increased ANGPT2

a. P10 cerebellum sections for CD31 with NG2 (top: 10×; bottom: 40×) and connexin-43 (CX43) co-staining, respectively. **b.** P10 cerebellum sections for staining of CD31 with VE-cadherin or claudin-5. The boxed areas are shown in high power for VE-cadherin and CD31 staining. Representative images of normal vessels (arrowheads), CCM lesions (asterisks) and vessels between lobules (arrows) are shown. **c**. Quantifications of coverages of NG2, CX43, VE-cadherin and claudin-5 on CD31 vessels. **d**. ANGPT2 and CD31 staining in P5 and P10 cerebellum sections. Representative high power images of ANGPT2-positive vessels are from boxed areas of P5 cerebellum. **e.** Cerebellum, retina and lung tissues as well as blood from WT and *Ccm3*$^{\text{ECKO}}$ pups were collected. Protein levels of ANGPT2 were determined by ELISA. **f–g.** mRNA levels (**f**) and protein levels (**g**) of ANGPT2-TIE2 pathway in cerebellum were determined by qRT-PCR and Western blotting. Data represent fold changes with WT levels normalized to 1.0. **h–i.** ANGPT2-pTIE2 was upregulated in human CCM lesions. Human CCM specimens were immunostained for CD31 with ANGPT2 or p-TIE2 (**h**) or Claudin-5 (**i**). Representative images from one (#2) of 8 human CCM3 samples are shown. Arrowheads indicate normal vessels whereas asterisks indicate for lesions. Arrows indicate gain of ANGPT2/p-TIE2 staining but loss of claudin-5 in lesions. n=10, *P <0.05,

P <0.01 (unpaired two-tailed Student's t-test). Error bars indicate s.e.m. Scale bar: **a (top): 100 μm; others: 25 μm (yellow); 5 μm (white for boxed images).

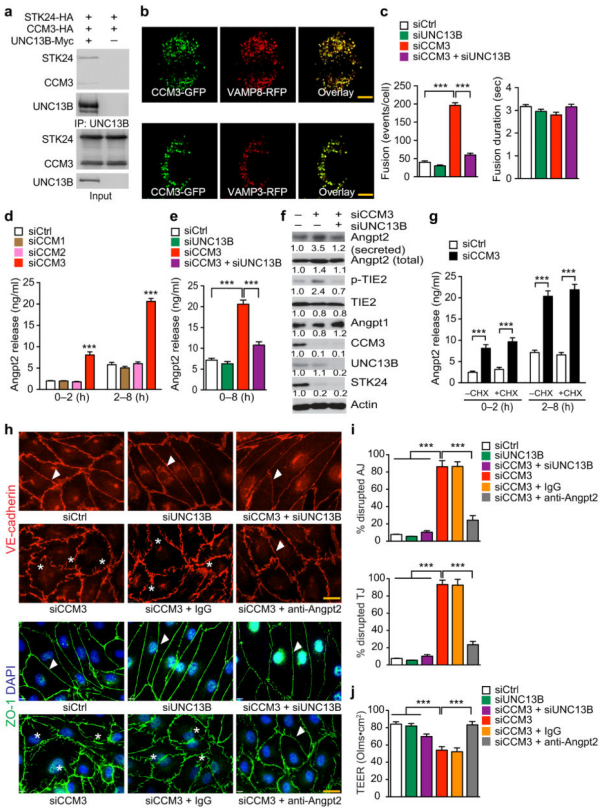

Fig.3. CCM3 restrains ANGPT2 release from ECs and maintains EC junctions

a. UCN13B forms a complex with CCM3 and STK24. Association of UNC13B with CCM3-STK24 was determined by co-immunoprecipitation with anti-Myc (UNC13B) followed by Western blotting with anti-HA for CCM3 and STK24. **b.** Co-localization of CCM3-GFP and VAMP8-RFP or VAMP3-RFP expressed in HBMVECs after transient transfection. Representative images were shown for 1 of 10 cells examined. **c.** CCM3-deficiency increases basal exocytic fusion events (but not fusion duration) which were rescued by co-silencing UNC13B. n=10, $^{**}P$<0.01 (one-way ANOVA). **d–g.** CCM3 regulates ANGPT2 secretion in ECs. HBMVECs were transfected with siRNAs for 72 hours followed by treatment with CHX (in panel **g**) for 2–8 h. ANGPT2 levels in media were determined by ELISA. Secreted ANGPT2 and intracellular proteins were detected by Western blotting. Data in panel **f** represent fold changes with control siRNA normalized to 1.0. n=6, $^{**}P$ <0.01 (two-way ANOVA in panels **d** and **g;** one-way ANOVA in panel **e**). **h–j**. CCM3-ANGPT2 axis regulates EC junctions and permeability. A control IgG or ANGPT2 neutralizing antibody (10 μg/ml) was added to HBMVECs at 16 h post-transfection with siRNAs. EC adherens junctions (AJ) and tight junctions (TJ) (**h**) were visualized by immunostaining, and percentages of disrupted junctions are quantified in panel **i** (counting 100 microscope fields in each group). **j**. Barrier function of ECs cultured on fibronectin-coated ECIS cultureware was assessed for transendothelial electric resistance (TEER; expressed as OLMS multipled by cm^2) by electrical cell-substrate impedance sensing. All experiments were repeated twice. Error bars indicate s.e.m., n=12. $^{**}P < 0.01$ (one-way ANOVA). Scale bar: **b** and **h**: 20 μm.

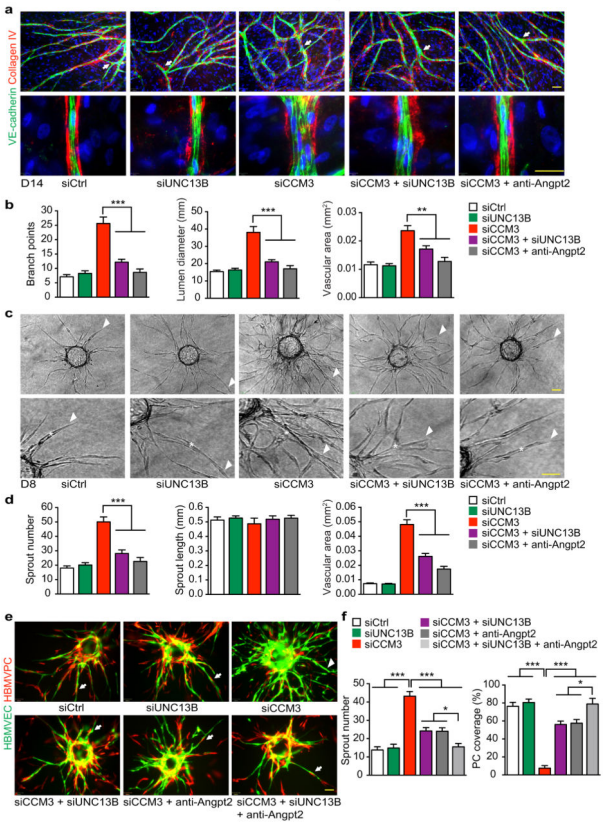

Fig.4. CCM3 maintains normal EC lumen formation and EC-PC associations

a–b. Organotypic angiogenesis assay. HBMVECs were transfected with siRNAs. 24h after transfection, cells were seeded onto a confluent layer of fibroblasts and were co-cultured for 14 days in the absence or presence of anti-ANGPT2 (10 μg/ml). EC sprouts and lumens were visualized by VE-cadherin and collagen IV staining. Branches are indicated by arrows. A representative high power confocal image for tubule lumen from each group is shown (**a**). Number of branch point, mean lumen diameter and lumen areas are quantified (**b**). **c–d.** 3D spheroid sprouting assay. siRNA-transfected HBMVECs were coated with microbeads, embedded in fibrin gels and grown in EGM2 medium for 8 days. A representative image of 10 beads for each sample is shown with sprouts and lumens indicated by arrowhead and asterisk, respectively. Quantifications of sprout number, sprout length and lumen areas are shown in panel **d**. **e–f.** EC-PC interactions in 3D spheroid sprouting assay. HBMVECs were infected with EGFP-expressing retroviruses and HBMVPCs were infected with mCherry-expressing lentiviruses. ECs were further transfected with siRNAs. ECs and PCs (2:1 ratio) were seeded to beads and treated as described in panels **c**–**d**. EC sprouts and PC coverage were visualized. A representative image of 10 beads for each sample is shown in panel **e** and % PC coverage of sprouts are quantified in panel **f**. n=10, *P<0.05; **P<0.01 (one-way ANOVA). Additional two independent experiments were performed. Error bars indicate s.e.m. Scale bar: 100 μm.

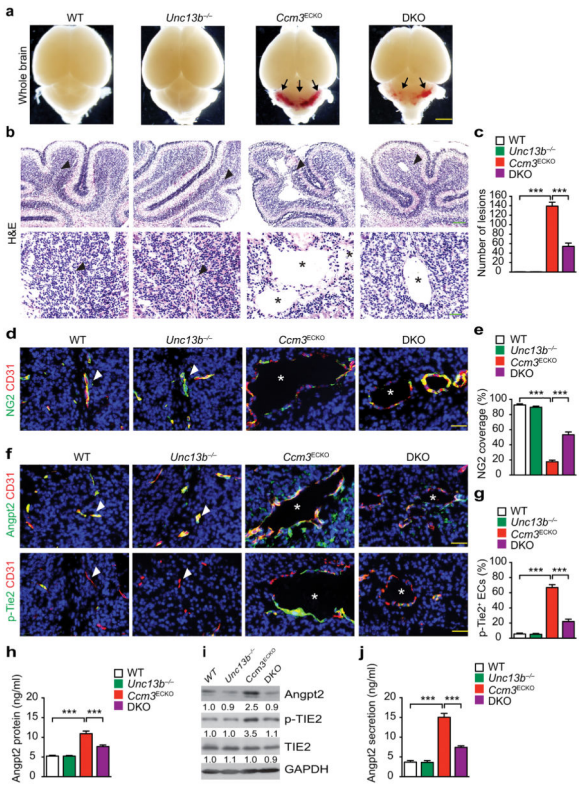

Fig.5. UNC13-deficiency rescues CCM phenotypes in *Ccm3*^{ECKO} mice

WT (*Pdcd10*$^{fl/fl}$), *Unc13b*$^{-/-}$, *Ccm3*^{ECKO} (Cdh5CerERT2;*Pdcd10*$^{fl/fl}$) and DKO (*Ccm3*^{ECKO};*Unc13b*$^{-/-}$) pups were fed with tamoxifen from P1 to P3 to induce deletion of CCM3. Cerebella were harvested at P10, and frozen sections were stained as indicated. **a**. Images for fresh brain tissue. Arrows indicate lesions. **b–c**. H&E staining and lesion quantifications. **d–e**. Co-staining for NG2 with CD31 and quantification of NG2^{+} coverage on microvessels. **f–g**. Co-staining for ANGPT2 with CD31 and p-TIE2 with CD31 and quantification of p-TIE2-positive ECs. Arrowheads indicate normal vessels and asterisks indicate lesions. **h–i.** Brain tissues were collected and ANGPT2 levels were determined by ELISA (**h**) and by Western blotting (**i**). **j**. Mouse brain microvascular ECs were isolated and ANGPT2 secretion from culture supernatants was measured by ELISA. n=10, *P <0.05; **P <0.01 (one-way ANOVA). Error bars indicate s.e.m. Scale bars: **a**: 2 mm; **b** (top): 400 μm; **b** (bottom), **d**, **f**: 100 μm.

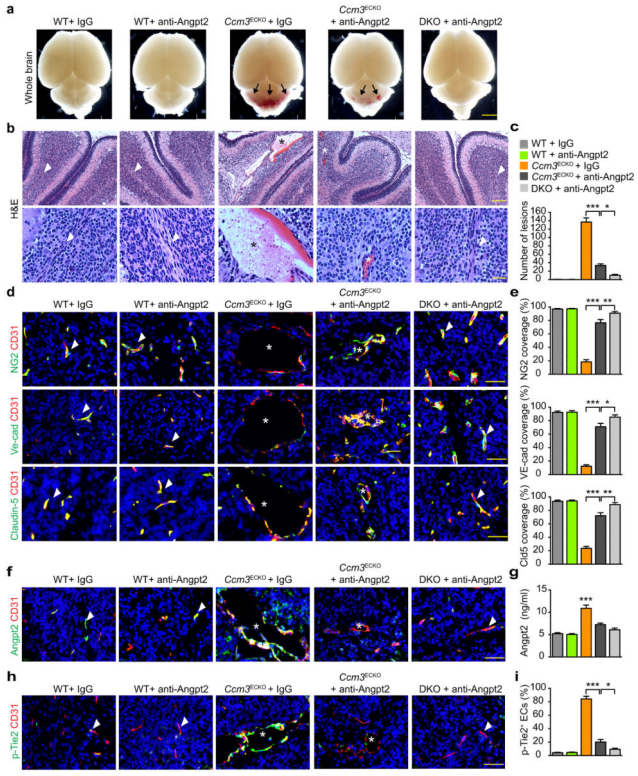

Fig.6. ANGPT2 neutralizing antibody blunts CCM lesion progression in *Ccm3*^{ECKO} mice

WT, *Ccm3*^{ECKO} and DKO (*Ccm3*^{ECKO};*Unc13b*$^{-/-}$) pups were fed with tamoxifen from P1 to P3 to induce CCM3 deletion. Pups were intraperitoneally injected with control IgG or ANGPT2 neutralizing antibody (10 μg/g body weight) from P2 and every other day thereafter. Cerebella were harvested at P10 in frozen sections. **a**. Images for fresh brain tissue. Arrows indicate lesions. **b–c**. H&E staining and lesion quantifications. **d–e**. Co-staining for NG2 with CD31, VE-cadherin with CD31 and Claudin-5 with CD31, and quantifications of NG2, VE-cadherin and Claudin-5 coverage on microvessels. **f**. Co-staining for ANGPT2 with CD31. **g.** Brain tissues were collected and ANGPT2 levels were determined by ELISA. **h–i**. Co-staining for p-TIE2 with CD31 and quantification of p-TIE2-positive ECs. Arrowheads indicate normal or normalized vessels and asterisks indicate lesions. n=10, *P <0.05, **P <0.01 (one-way ANOVA). Error bars indicate s.e.m. Scale bars: **a**: 2 mm; **b** (top): 400 μm; **b** (bottom), **d**, **f, h**: 100 μm.